

**RESEARCH ARTICLE**

Evaluation of a simple analytical model for offshore wind farm wake recovery by in situ data and Weather Research and Forecasting simulations

Andreas Platis¹ | Marie Hundhausen¹ | Moritz Mauz¹ | Simon Siedersleben² | Astrid Lampert³ | Konrad Bärfuss³ | Bughsin Djath⁴ | Johannes Schulz-Stellenfleth⁴ | Beatriz Canadillas^{3,5} | Thomas Neumann⁵ | Stefan Emeis² | Jens Bange¹

¹Environmental Physics, GUZ, University of Tübingen, Tübingen, Germany

²Institute of Meteorology and Climate Research, Atmospheric Environmental Research (IMK-IFU), Karlsruhe Institute of Technology, Garmisch-Partenkirchen, Germany

³Institute of Flight Guidance, Technische Universität Braunschweig, Braunschweig, Germany

⁴Institute of Coastal Research, Helmholtz Zentrum Geesthacht, Geesthacht, Germany

⁵Renewable, UL International GmbH, Oldenburg, Germany

Correspondence

Dr. Andreas Platis, Environmental Physics, GUZ, University of Tübingen, Tübingen, Germany.
Email: andreas.platis@uni-tuebingen.de

Present address

Dr. Andreas Platis, Eberhard Karls Universität Tübingen Environmental Physics Group, ZAG Schnarrenbergstr. 94-96 72076 Tübingen / Germany

Funding information

German Federal Ministry for Economic Affairs and Energy (Bundesministerium für Wirtschaft und Energie), Grant/Award Number: FKZ 0325783

Abstract

The recovery of offshore wind farm wakes in the German Bight was analyzed by a unique in situ data set, measured on-board the research aircraft Dornier Do-128 during the WIPAFF project in 2016 and 2017. These observations were used to validate a simple analytical wake recovery model in five case studies. The observed recovery rates were compared with the results of the mesoscale Weather Research and Forecasting (WRF) model. The airborne data show that the wake recovery can be described by an exponential function as expected by the analytical model and strengthens the hypothesis that the vertical downward momentum flux has an important influence on the wake recovery. However, the predicted wake recovery rates (by the analytical model) do not always fully agree with the observations. Although, as a first-order approximation, the model seems to perform well, further optimization has to be implemented to account for wind park layout, turbine induced turbulence, and horizontal momentum flux. WRF simulations reveal an exponential recovery, although the mesoscale model does not reproduce the correct atmospheric conditions for most of the cases. Therefore, the wake recovery rates estimated by WRF disagree with the measured data in most of the studied cases.

KEYWORDS

airborne measurements, analytical model, offshore, wake recovery, wind energy, wind farm density, WRF

1 | INTRODUCTION

In 2019, wind energy turbines produced 24.4% of the gross electricity in Germany with an installed capacity of 60.9 GW.¹ In the German North Sea and Baltic Sea, 7.7 GW offshore wind energy has been installed so far until July 2020.² Compared to installations on land, the large potential of offshore deployments is based on higher wind speeds over the ocean and a lower level of turbulence. Moreover, the sea provides large unused areas³ and a reduced noise or visual impact on the public.⁴ For an optimal area use and in order to minimize costs for infrastructure, offshore wind turbines are clustered into large wind farms with an extent of several tens of kilometers.⁵

As each turbine extracts kinetic energy, a region downstream of the wind farm builds up, where the wind speed is reduced (ideally down to 1/3 of the undisturbed wind speed according to the classic theory of Betz from 1926), the so called wake. At the edges of this zone, there is an increased level of turbulence.^{6,7} The extension of wakes depends on the mixing within the atmosphere. Hence, wakes are expected to be especially large at offshore locations, where a low surface roughness leads (in general) to low turbulence intensities that inhibit the dissipation of the wake. It is expected that the length of wind farm wakes increases with increasing atmospheric stability.³ Satellite images⁸⁻¹⁰ as well as first in situ measurements show that offshore wakes exceed several tens of kilometers in the North Sea during stable atmospheric conditions.^{7,11}

With such large wake extensions, wind farms significantly impact and decelerate the flow field. This implies that lower energy production is achieved at wind farms located downstream. Therefore, the understanding and modeling of wind-farm wakes is of significant concern for the successful planning of future wind-farm clusters in the German Bight.

Basically, two types of model implementations capturing the effect of wind farms can be distinguished. On the one hand, there is the bottom-up approach. This means that the impact of the single turbine is examined and the effect of the turbine cluster is obtained by superposition.¹² However, this approach requires a good understanding of the single turbine wake as well as an appropriate “wake superposition method.”^{13,14} When it comes to large wind farms, as today's offshore installations, the approach becomes increasingly complicated. Therefore, for large offshore wind farm clusters, it may be advantageous to model the wind farm as a whole, with the so called top-down models.^{15,16} In this second model class on the other hand, the farm is parameterized and implemented as an additional surface roughness, a sink of momentum, or as a gravity-wave generator.^{17,18}

Recent studies with numerical simulations using the Weather Research and Forecasting (WRF) model have reproduced these wakes in the far field of offshore wind farm sites and show good agreement with observations.^{7,19,20} Here, WRF acts as a top-down model by parameterizing the wind turbines within one grid cell as a whole. All these studies used the wind farm parameterization of Fitch et al.²¹ With the mesoscale resolution, WRF is a suitable tool to study the far field downstream of larger wind farm clusters. However, although computational power is easily accessible, these days, mesoscale simulations are still computationally expensive. Remedy for this can be a simple analytical approach to evaluate wakes and plan wind farm clusters.^{18,22,23} This study will focus on such a model introduced by Emeis,²³ (hereafter E10), which considers atmospheric stability and is based on an exponential wake recovery approach. With the E10, modeled wake lengths of 10 km for strongly convective conditions and wakes exceeding 40 km during very stable conditions are obtained for a theoretical offshore site.²³

Within this study, the wake characteristics of offshore wind farm wakes are evaluated with the airborne data set collected during the WIPAFF project.⁷ This study carries out a detailed validation of the E10 model, and the predictions from the E10 model are compared with the airborne in situ data and mesoscale simulations.

In Section 2, a brief summary of the analytical E10 model is given. In Section 3, an overview of the WIPAFF campaign is given and the data analysis is explained. In Section 4, results of five case studies are described with a subsequent discussion and summary in Section 5 and a conclusion in Section 6.

2 | WAKE RECOVERY ACCORDING TO THE ANALYTICAL MODEL

In order to estimate the wind speed reduction at hub height behind large, offshore wind farms, the following approach was introduced by Emeis,²³ called E10 hereafter. Under the assumption that the upwind wind farm is infinitely large, the missing momentum, here downstream of the farm, is compensated with time by the turbulent vertical momentum flux τ from aloft:

$$\frac{\partial u_r}{\partial t} = \frac{\partial \tau}{\partial z}, \quad (1)$$

where u_r is the reduced wind speed downstream of the wind farm at hub height h , ρ the air density, and z is the height above ground or sea.

A complete derivation and a detailed description of the E10 model can be found in Emeis.^{17,23} The advantage of the model is that the temporal behavior of the reduced wind speed $u_r(t)$ in the wake downstream of a wind farm is described in a single equation and depends on the initial wind speed deficit u_{r1} (observed directly downstream of the wind farm) and the stability of the atmosphere represented by the friction velocity,

which will be further explained in more detail in Section 3.3. Note that the wind park density is therefore included in the model by u_{r1} , since u_{r1} depends on the park density itself. The wind deficit decreases exponentially with the wake recovery rate α :

$$u_r(t) = u_f(t) + (u_{r1} - u_f(t)) \exp(-\alpha t), \quad (2)$$

where u_f is the undisturbed (free) wind speed outside the wake. The wake recovery rate α is described.

$$\alpha = \frac{K_m}{(\Delta z)^2} = \kappa u_* \frac{z_f}{(\Delta z)^2}, \quad (3)$$

where K_m is the turbulent momentum exchange coefficient, which can be approximated by $K_m = \kappa u_* z_f$ with $\kappa = 0.4$ being the von Kármán constant and u_* the friction velocity. The height $z_f = h + \Delta z$ describes the height at which the undisturbed wind speed is reached above the wind farm. Consequently, Δz is the height difference between the hub height and the undisturbed flow top of the rotor blades.

Finally, Equation (2) can be expressed by the ratio R_r between the wind speed u_r in the wake and the undisturbed wind speed u_f outside the wake.

$$R_r(t) = \frac{u_r(t)}{u_f(t)} = 1 - \left(1 - \frac{u_{r1}}{u_f(t)}\right) \exp(-\alpha t). \quad (4)$$

3 | METHOD

3.1 | WIPAFF campaign

The study is based on airborne meteorological measurements in the German Bight conducted in the research project WInd Park Far Field (WIPAFF). Five field campaigns were carried out from September 2016 to October 2017, comprising 41 measurement flights in total. An overview of all flights can be found in Platis et al.⁷ The measurements were performed with the research aircraft Dornier Do-128 of the Technische Universität of Braunschweig. It is equipped among others with sensors for temperature, humidity, pressure, and wind components, sampling with a frequency of 100 Hz. Details about the measurement devices can be found in Corsmeier et al.²⁴ and Lampert et al.²⁵ The airspeed of the aircraft during the measurements flights was 66 m s^{-1} .

All measurement flights were conducted over the North Sea. An overview of all analyzed flights for this study is given in Table 1. They were performed in the vicinity of the operating offshore wind farm cluster Amrumbank West, Nordsee Ost, Meerwind Süd/Ost (AW/NO/MSO); see Figure 1. Only those flights were analyzed that exhibit a well-developed wake and were accompanied by WRF simulations for the respective case study. A typical flight comprises the following features: The take-off and landing was at the German coast at one of the airports Wilhelmshaven, Borkum or Husum. In the vicinity of the wind farm cluster, vertical profiles of the lower atmosphere from 30 - 500 m were measured to determine the thermal stability. Downstream of the wind farm cluster, a so called meander pattern was flown (visualized by the black line in Figure 2). While the first leg has a distance of about 1 km to the farm, the farther downstream legs follow with a spacing of 10 km. The number of consecutive legs was adjusted to the observed wake for each flight but was limited by the flight endurance. The altitude of the flights was 100 m above sea level, which is the turbine hub height of the respective wind farms.

TABLE 1 Overview of all flights used in this study

Flight No.	Date	Take off in UTC	Landing in UTC	Thermal Stability	WS in m s^{-1}	WD in $^\circ$
7	2016-09-10	07:33	11:15	slightly stable	8.5	190
24	2017-05-27	08:35	11:58	stable	10.0	150
25	2017-05-27	12:31	16:36	stable	12.0	130
30	2017-08-08	08:34	12:33	slightly stable	10.0	85
31	2017-08-08	12:59	17:07	stable	15.0	80

Note. The Flight No. is according to the total numbering of all flights during the WIPAFF campaigns in 2016 and 2017.^{7,25} Thermal stability represents the atmospheric stratification.

Abbreviations: WD, wind direction; WS, wind speed.

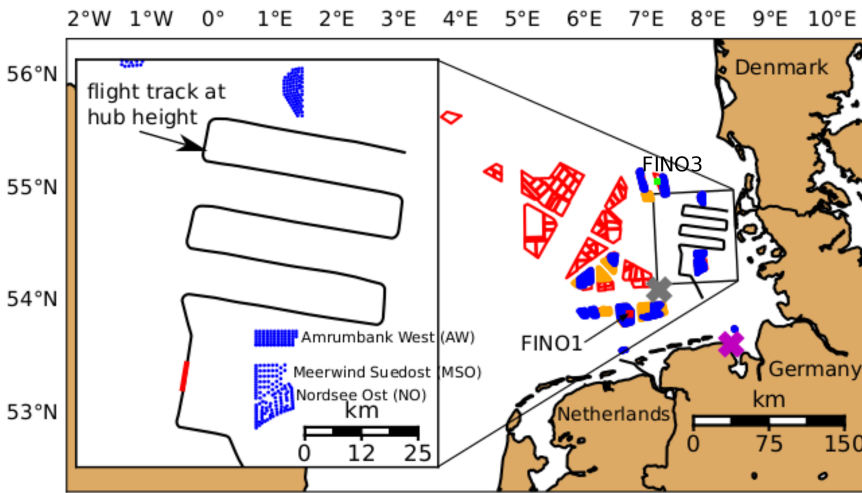


FIGURE 1 Positions of offshore wind farms in the German Bight as of December 2017. Blue regions are farms that were in operation, and red regions indicate farms still in the approval process. Orange regions are those wind farms that are under construction. The purple cross indicates the take-off airport Wilhelmshaven, and the red box indicates the location of the FINO1 measurement tower and the green box of FINO3. The red line along the flight path in the left figure marks the track where the vertical profile was measured. The map is adapted from the data of the German Federal Maritime and Hydrographic Agency (BSH) and copied from Platis et al.⁷ [Colour figure can be viewed at wileyonlinelibrary.com]

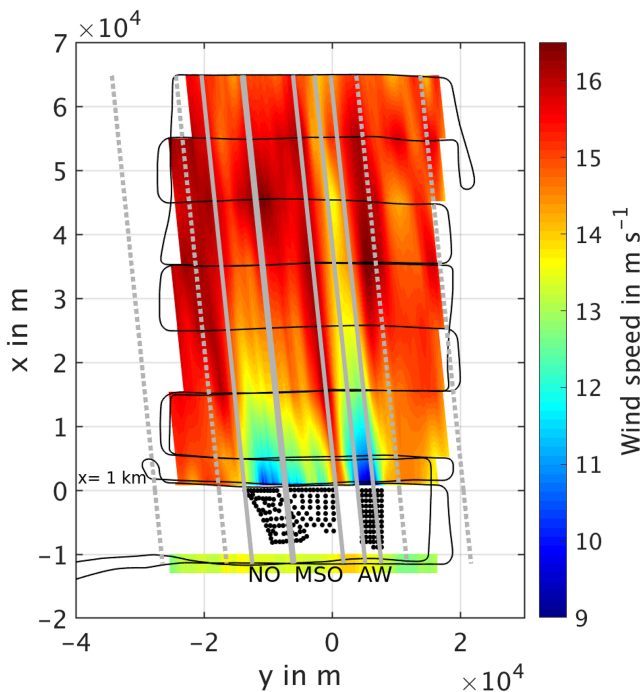


FIGURE 2 Contour plot of the interpolated wind field along the mean wind direction, measured during the Flight 31 on August 8, 2017. The orientation of the plot is west, and the mean wind direction is east. The black line indicates the flight track. The black dots indicate the wind turbines. The undisturbed wind field (outside the wake) is indicated by gray dashed lines and the wake boundaries by gray solid lines. The wind parks are Amrumbank West, Nordsee Ost, Meerwind Süd/Ost (AW/NO/MSO). At $x = 1$ km, the initial wind speed deficit D_{r1} is measured inside the wake [Colour figure can be viewed at wileyonlinelibrary.com]

For the estimation of the friction velocity u_* in the marine boundary layer, sonic data from the research mast FINO1 at 40 m above the sea surface was used. FINO1 is a meteorological measurement tower located about 45 km offshore, north of the German Island Borkum in the German Bight (see Figure 1) and is equipped among others with 20 Hz high frequency sonic anemometers.²⁶ Further, mean temperature and wind data at several heights from FINO1 and FINO3 (a second measurement tower located north of the wind farm AW) is used for vertical profiling of the lowest boundary layer between the sea surface and 100 m.

3.2 | Wake characterization

The data source for the wake characterization are the wind speed measurements obtained during the meander pattern measured at hub height. The flight path is transferred from the GPS reference coordinate system to a Cartesian system with x (along the flow) and y -coordinates (perpendicular to the flow) in meters and rotated in the mean wind direction (wind is coming from negative x). An example is given in Figure 2. In this contour-plot figure, a linear interpolation along the mean wind direction is done.

The first step of the wake characterization is to determine the wake region. This is done manually, choosing a left and a right boundary of the wake directly downstream of the wind farm within which the wind speed is significantly reduced. In the example, distinct wakes build up behind the three different wind farms AW/NO/MSO in the cluster; thus, several wake areas are defined. The wake region is then extended linearly along the mean wind direction (Figure 2).

In the next step, the undisturbed zone is defined left and right of the wake using a distance of at least 4000 m as buffer zone between wake and undisturbed area. In this zone, the undisturbed wind speed $u_f(x)$ was measured.

The extent of the wake is then defined by the ratio $R_r(x)$ according to Equation (4) but for the spatial domain. $u_r(x)$ is the wind speed in the wake zone calculated as arithmetic mean for each leg and thus at different distances x to the wind farm. $u_f(x)$ is the mean wind speed in the undisturbed zone on both sides of the wake. It should be noted that different from the E10-Theory, $u_f(x)$ varies along x as well. Similar to the methodology by Christiansen and Hasager⁸ and Djath et al,¹⁰ the decision of a variable undisturbed wind speed u_f was made because of significantly heterogeneous wind fields in the data due to mesoscale effects. The maximum length of a wake is defined at the downstream distance at which the recovery R_r reaches 95%. The wind speed deficit D is obtained by

$$D(x) = 1 - R_r(x). \quad (5)$$

For the first leg downstream of the wind farm located at the distance $x = 1$ km, this leads to the initial wind speed deficit D_{r1}

$$D_{r1} = 1 - R_r(1\text{km}) = 1 - \frac{u_{r1}}{u_{f1}}. \quad (6)$$

The E10 theory describes the wake recovery in the time domain in terms of a wake duration. As the flight data are measured in the spatial domain x , the x -axis is transferred into the time domain t with the relationship

$$t = \frac{x}{u_r}. \quad (7)$$

With this, the ratio of Equation (4) is obtained where \bar{u}_r is the mean wind speed within each wake averaged over all legs. For simplicity, the time domain index t for the recovery rate α is skipped hereafter.

For a better overview, all important variables are summarized in Table 2 with their corresponding meaning.

3.3 | Calculation of wake recovery coefficient α by E10

The theoretical value of α is validated according to the theory of the exponential wake recovery by E10. Recalling the definition of Equation (3), the following terms have to be defined: first, $\frac{z_f}{(\Delta z)^2}$ describing the ratio between the height z_f of undisturbed wind speed and its vertical separation

TABLE 2 Overview of all important variables used in this study

Variable	Meaning
h	Hub height
z_f	Height of the undisturbed (free) flow
Δz	Height difference between h and z_f
u_r	Reduced wind speed downstream of the wind farm inside the wake at h
u_f	Undisturbed (free) wind speed outside of the wake at h
u_{r1}	Initial reduced wind speed downstream (at $x = 1$ km) of the wind farm (inside the wake) at h
u_{f1}	Initial undisturbed wind speed downstream (at $x = 1$ km) of the wind farm (outside the wake) at h
D_{r1}	Initial wind speed deficit at $x = 1$ km at h
R_r	Ratio of u_r / u_f
α	Wake recovery rate
α_{obs}	Wake recovery rate observed by the airborne data
α_{WRF}	Wake recovery rate by the WRF model
α_{FINO}	Wake recovery rate calculated by E10 with $u_{* \text{FINO}}$
α_{profile}	Wake recovery rate calculated by E10 with $u_{* \text{profile}}$
u_*	Friction velocity
$u_{* \text{FINO}}$	Friction velocity calculated by the FINO1 data (Equation 8 "direct method")
$u_{* \text{profile}}$	Friction velocity calculated by the "profile method" (Equation 9)

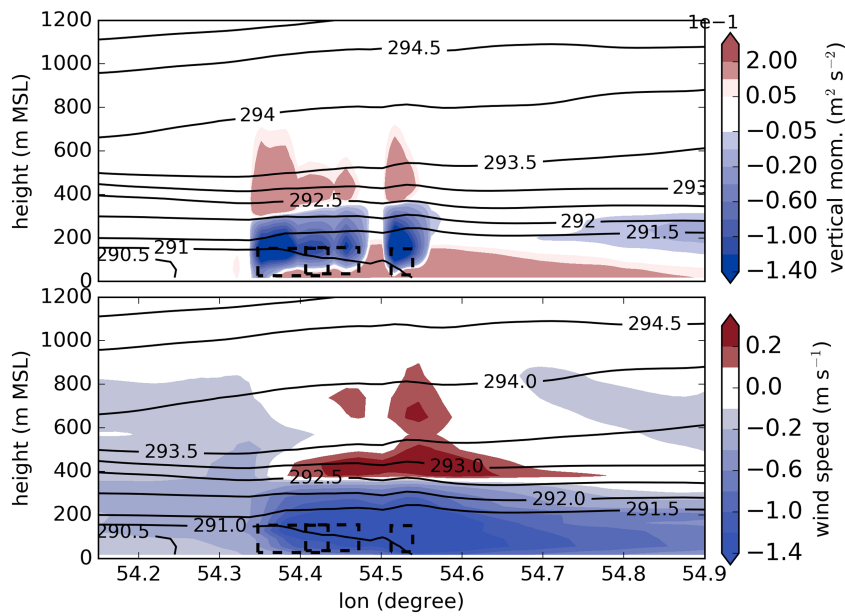


FIGURE 3 Cross-section of the vertical momentum flux (top) and wind speed (bottom) by the WRF run for case study 7, 09:00 UTC alongside the mean wind direction from left to the right (southerly wind). The black dashed rectangles mark the wind farms Meerwind Süd/Ost (MSO), Nordsee Ost (NO), and Amrumbank West (AW) from left to right [Colour figure can be viewed at wileyonlinelibrary.com]

TABLE 4 Overview of the wake recovery rates and friction velocities for each case study

Flight No.	wind farm	u_{*FINO} $m s^{-1}$	$u_{*profile}$ $m s^{-1}$	α_{FINO_D} h^{-1}	$\alpha_{FINO_{WRF}}$ h^{-1}	$\alpha_{profile_D}$ h^{-1}	$\alpha_{profile_{WRF}}$ h^{-1}	α_{obs} h^{-1}	Δz_{WRF} m
7	MSO/NO/AW	0.21	0.28	4.59	0.94	6.16	1.26	1.26	400
24	MSO/NO/AW	0.28	0.35	6.11	1.78	7.70	2.24	0.90	300
25	MSO/NO	0.33	0.44	7.28	1.29	9.68	1.72	1.26	450
25	AW	0.33	0.44	7.28	1.29	9.68	1.72	0.96	450
30	MSO	0.22	0.26	4.73	2.32	5.72	2.81	4.26	200
30	NO	0.22	0.26	4.73	2.32	5.72	2.81	2.76	200
30	AW	0.22	0.26	4.73	2.32	5.72	2.81	1.26	200
31	MSO	0.29	0.08	6.48	3.18	1.76	0.86	3.60	200
31	NO	0.29	0.08	6.48	3.18	1.76	0.86	6.60	200
31	AW	0.29	0.08	6.48	3.18	1.76	0.86	1.80	200

Note. α_{obs} is obtained by the airborne data. α_{FINO} and $\alpha_{profile}$ are calculated by the E10 model using either the friction velocity u_{*FINO} by the FINO1 measurements or $u_{*profile}$ by the profile method. The additional index D or WRF at α_{FINO_D} and $\alpha_{profile_D}$ indicates which Δz by E10 was used to estimate the separation height. D refers to a height of 125 m which approximately equals the rotor diameter of the wind farm Amrumbank West (AW), Nordsee Ost (NO), and Meerwind Süd/Ost (MSO). Δz_{WRF} is the separation height estimated by the WRF model for each case study.

Δz to hub height h , squared. As no empirical values for z_f (or Δz) are available, and no recording of vertical profiles of the wind speed in and above the wind farm was possible during the measurements flights, the cross-section of the turbulent momentum flux and the wind field modeled by the WRF simulation are used (see more details in Section 3.4) for the respective cases.

To make the influence of the vertical momentum flux and the change of the flow by the wind farm apparent, an example is illustrated for the WRF model run of Flight 7 (Figure 3). It shows the difference between a control run without the wind farm cluster and a run with the wind farm cluster implemented. A significant change in the downward flux and in the wind field up to an altitude of 500 m is evident, implying a separation height Δz_{WRF} of 400 m. The index “WRF” highlights that the estimation is done by the WRF runs, hereafter. For the other runs, the information of Δz_{WRF} is included in Table 4.

Two approaches were applied to obtain the shear or friction velocity u_{*} , required in Equation (3):

- Direct method: the calculation of u_{*} by the vertical fluxes of horizontal momentum (i.e., the wind-speed covariances)²⁷ using sonic FINO1 data of the wind speed components u, v, w :

$$u_{*FINO} = \left((\overline{u'w'})^2 + (\overline{v'w'})^2 \right)^{\frac{1}{4}}. \quad (8)$$

- Profile method: Assuming a logarithmic wind profile and considering the stability,²⁷ u_* is obtained from

$$u_{*profile} = \frac{u_f(z)\kappa}{\left[\ln\left(\frac{z}{z_0}\right) + \Psi\left(\frac{z}{L}\right) \right]}, \quad (9)$$

where L is the Obukhov length,²⁷ $\Psi\left(\frac{z}{L}\right)$ is the stability function according to Paulson²⁸ and Högström,²⁹ and $z = h$ is the height of the upstream flight leg located in the undisturbed flow at hub height. The stability correction in $\Psi\left(\frac{z}{L}\right)$ is estimated using the observed z/L by the undisturbed leg. Moreover, the roughness length is set to $z_0 = 0.0001$ m which is common for the sea surface during moderate wind speeds between 10 and 15 m s^{-1} according to Charnock³⁰ and Garratt.³¹ All values of u_* are included in Table 4.

3.4 | WRF simulation

The mesoscale simulations were performed with the WRF model (version 3.8.1). Three domains were used, with a 15-km horizontal resolution in the coarsest followed by two domains with 5 and 1.6 km. The wind farms in the mesoscale simulations were represented by the wind farm parameterization of Fitch et al.²¹ interacting with the boundary layer scheme of Nakanishi and Niino.³² The boundary conditions were provided by ERA5 data. This model setup is identical to the one used in Siedersleben et al.^{20,33,34} Therefore, the interested reader is referred to these three articles for full details. To evaluate the analytical wake model E10 by the WRF simulation, analogously to the flight measurements, data have to be processed first. The model output is transferred to x - and y -coordinates in meters using the same origin as for the according flight measurements. Next, the output of wind speed at hub height is linearly interpolated to a grid with a spacing of 100 m in x - and y -direction. Then the procedure is the same as for the flight evaluation: first, the boundaries of the wake and the undisturbed zone are chosen. Second, $u_r(x)$ and $u_f(x)$ are evaluated, and finally, the wake recovery is expressed in terms of R_r and transferred to the time domain.

4 | RESULTS

In this section, the five case studies are analyzed, as listed in Table 1, to compare the in situ results of the wake recovery with the E10 model and with WRF simulations.

The detailed analysis of the case studies comprises three parts:

- an overview about the synoptic and atmospheric conditions
- a characterization of the wake by airborne measurements and WRF simulations
- a comparison of the measurements and simulations to the analytical model

The two flights (no. 30 and no. 31) on August 8, 2017, comprise similar wind directions and flight patterns but different thermal stability conditions. Therefore, they are considered as exemplary cases to analyze the influence of a stability change from stable (Flight 31) to slightly stable (Flight 30) in detail.

4.1 | Flight 31—August 8, 2017, afternoon—with strong thermal stability

The synoptic situation during the measurement Flight 31 is a low pressure system approaching the German Bight at 12:00 UTC. For 12:00 UTC, its center is predicted over the Netherlands leading to easterly winds at the wind farm cluster AW/NO/MSO with a wind speed of about 15 m s^{-1} at hub height. However, with the North-Eastwards moving low pressure system, the wind direction turns to a southern and more variable direction at 18:00 UTC. According to the temperature profile measured in the vicinity of the wind farm cluster, a thermally stable layer was present up to approximately 100 m above sea level with a lapse rate of +1.24 K/100 m (see Figure 4). The hub height of the turbines of the wind farm cluster is around 100 m, with a rotor diameter of 120 m; thus, the total turbine height reaches 160 m. In this case, with the detected surface layer up to 100 m, the turbines are in the stable layer, but the rotor blades do cut into the neutral layer above. The situation is similar for NO and MSO.

4.1.1 | Flight data

During Flight 31 (13:59 UTC to 17:07 UTC), a 65 km long meander pattern behind the wind farm cluster AW/NO/MSO was measured (Figure 2). The contour plot reveals that the wakes of MSO and NO overlap, whereas downstream of AW, a distinct wake is observed. The measured wind

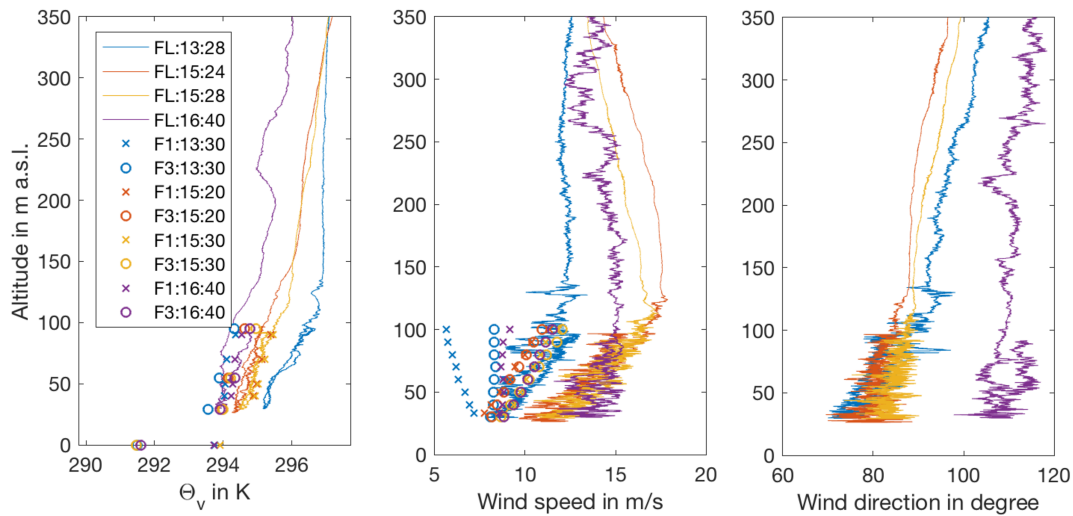


FIGURE 4 Vertical profile of virtual potential temperature (left), wind speed (middle), and wind direction (right), measured during Flight 31 in the vicinity of the wind farm AW/MSO/NO as shown in Figure 1. FL is the abbreviation for flight data, and F1 corresponds to FINO1 data and F3 to FINO3 data [Colour figure can be viewed at [wileyonlinelibrary.com](#)]

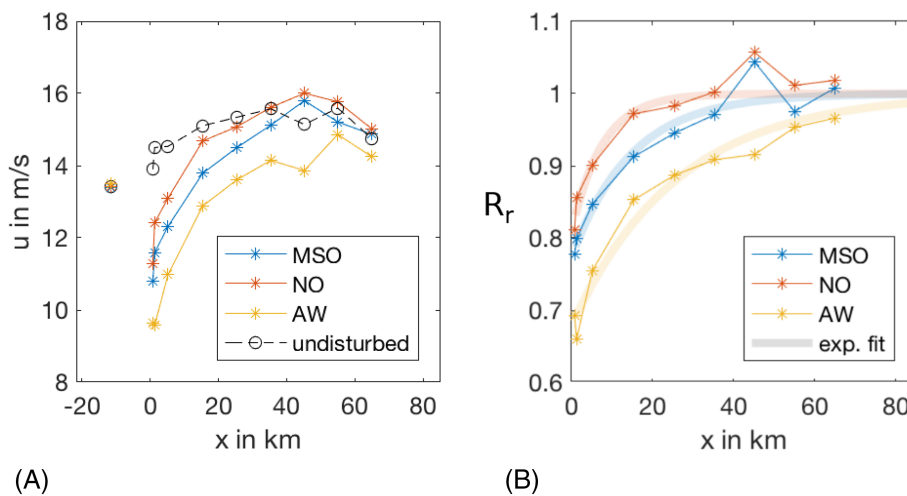


FIGURE 5 (A) Wind speed in the wake and undisturbed zone of Flight 31. The blue line indicates the wind speed in the wake downstream of the wind farm MSO, the red NO and the yellow one AW. The dashed black line indicates the wind speed of the undisturbed flow aside of the wake. (B) Relative wind speed deficit of Flight 31 [Colour figure can be viewed at [wileyonlinelibrary.com](#)]

speed in the wake and in the undisturbed flow is displayed in Figure 2. The wind speed in the undisturbed, upstream leg of the wind farm ($x = -11$ km) is homogeneous along the flight leg except for the section between AW and NO with higher wind speeds. This could be explained by a channel flow effect with an accelerated flow between the wind parks. Looking at the background mesoscale wind field, an overall acceleration from the undisturbed leg upstream to the downstream zone of about 2 m s^{-1} is measured.

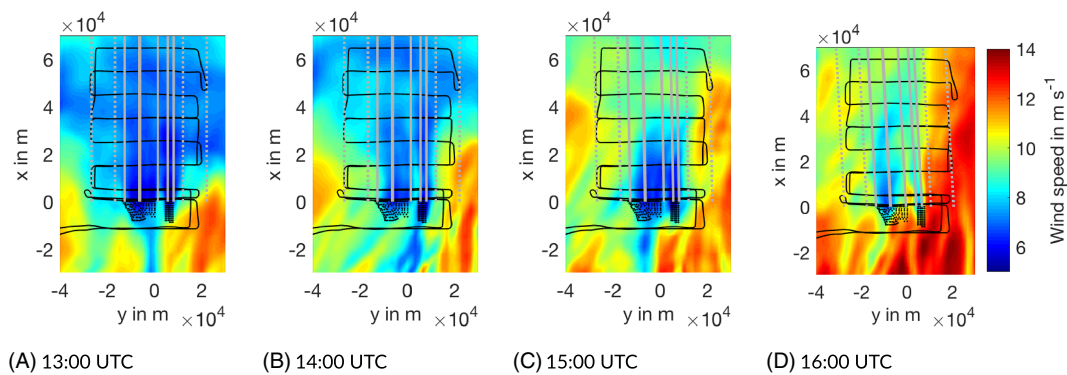
The recovery curve is shown in Figure 5B, where the ratio R_r between the wind speed in the wake and the undisturbed zone over the downstream distance x is plotted. The following wake parameters are determined: initial deficit D_{r1} at $x = 1$ km, wake length, and duration to 95% recovery. These parameters were determined for all three wind farms and are summarized in Table 3. The highest initial wind speed deficit of 31% and longest wake extension to 47 km or 62 min is observed behind the densest farm AW. The medium deficit (22%) and medium wake length (25 km) and duration (30 min) develops behind MSO with the medium turbine density of the three farms, respectively. And finally, the lowest deficit (19%) and shortest wakes with 12 km or 14 min are assigned to the cluster NO with lower wind turbine density.

Following the theory of the exponential wake recovery (Equation 4), an exponential function is fitted to the results. The parameters used for the fitting are the initial wind speed deficit D_{r1} and the recovery rate α as provided in Table 3. For better clarity, the recovery rate observed by the airborne measurements is represented with α_{obs} hereafter. The exponential function agrees well with the measured data as revealed by the fitted exponential curve in Figure 5B and by the low root mean square error (RMSE) of 0.6 to 1.2 between the fit and the measurements. α_{obs} ranges from 6.60 h^{-1} for NO to 1.80 h^{-1} for AW and decreases with the farm density. These results provide evidence that not only the initial wind speed deficit and wake extension but also the recovery rate α depend on the wind farm layout.

TABLE 3 Measured and fitted values of the wake parameters of Flights 31 and 30

	Flight measurement			Best fit	
	D_{r1}	x_{95} in km	t_{95} in min	α_{obs} in h^{-1}	RMSE
Flight 31					
MSO	22	25	30	3.6	1.2
NO	19	12	14	6.6	1.2
AW	31	47	62	1.8	0.6
Flight 30					
MSO	29	15	29	4.2	2.4
NO	19	21	40	2.8	2.4
AW	28	38	76	1.3	1.8

Note. Wake length x_{95} and duration t_{95} are evaluated at the point of 95% recovery. D_{r1} is the initial wind speed deficit measured at the distance $x = 1$ km downstream of the wind park. α_{obs} is the recovery rate in h^{-1} , and the RMSE describes the root mean square of the fitting.

**FIGURE 6** Wind speed contour plots and assigned wake boundaries of the WRF output for the case study of Flight 31 for different times of the simulation run [Colour figure can be viewed at wileyonlinelibrary.com]

4.1.2 | WRF simulation

The WRF output was analyzed hourly from 13:00 UTC to 16:00 UTC covering the flight time. The model outputs are hourly averaged. The profiles of virtual potential temperature by the WRF model agree with the measured stable thermal stratification, although the modeled temperature is slightly warmer. The transition from the stable surface layer to the residual layer above is smoother. Compared to the measurements, the wind speed by the WRF runs is underestimated by $1\text{--}2\text{ m s}^{-1}$. Analyzing the wind field and the recovery R_r (see Figures 6A–D and 7A–C), the WRF model overestimated the length of the wakes. This can be explained by the higher initial wind speed deficit D_{r1} . On average, D_{r1} for MSO is 33%, for NO 35%, and for AW even 40%.

By fitting an exponential function to the WRF results (Figure 6A–D), also the recovery rate α_{WRF} is underestimated and remains almost constant for the three farms with 0.96 h^{-1} for MSO and 0.78 h^{-1} for NO and AW. The fit error (with RMSE = 2.1) is higher than the one of the in situ data. The WRF model does not picture the observation for this case study properly as it simulates a lower initial wind speed deficit. Therefore, the recovery rates are higher compared to the observation and the analytical model as evaluated below.

4.1.3 | E10 model

For the calculation of the recovery rate by the E10 model, the same separation height of $\Delta z_{WRF} = 200\text{ m}$ assumed by the WRF model is used.

The friction velocity u_{*FINO} measured at FINO1 is 0.21 m s^{-1} . Thus, a recovery rate $\alpha_{FINO} = 3.18\text{ h}^{-1}$ is calculate by the E10 model. Using the calculated friction velocity by the profile method (Equation 9) with $u_{*profile} = 0.08\text{ m s}^{-1}$, a recovery rate $\alpha_{profile} = 0.86\text{ h}^{-1}$ is calculated by E10. This is 3.5 times smaller than using the FINO data. The question arises why there is such a difference between u_{*FINO} and $u_{*profile}$. For the calculation of $u_{*profile}$ according to Equation (9), the Obukhov length L is measured by the research aircraft at $z = 100\text{ m}$ above the sea surface. Remembering that the inversion height is at about 100 m in the case of the Flight 31 as well, L is not representative for the layer below. This leads to an underestimation of the friction velocity.

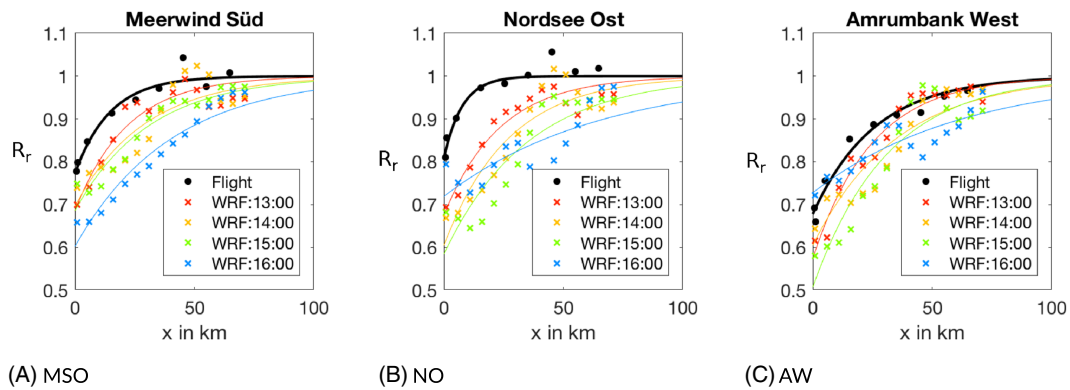


FIGURE 7 Relative wind speed R_r deficit in WRF behind the three wind farms MSO, NO, and AW for the case study of Flight 31. The solid line displays the best exponential fit of the airborne measurements. The red line shows the best fit of the WRF run at 13:00 UTC, the yellow at 14:00 UTC, green at 15:00 UTC, and blue at 16:00 UTC [Colour figure can be viewed at [wileyonlinelibrary.com](#)]

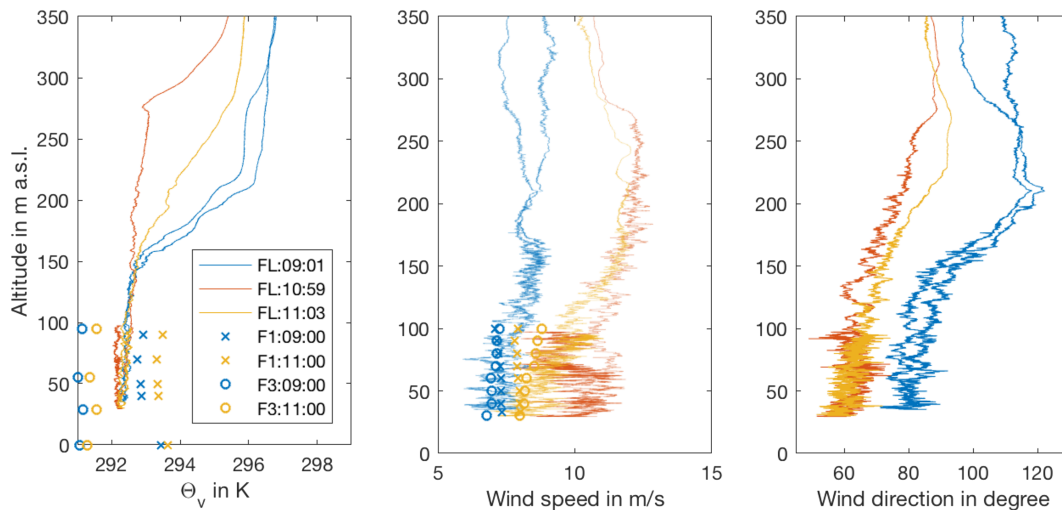


FIGURE 8 Vertical profile of virtual potential temperature (left), wind speed (middle), and wind direction (right), measured during Flight 30 in the vicinity of the wind farm AW/MSO/NO as shown in Figure 1. FL is the abbreviation for flight data, and F1 corresponds to FINO1 data and F3 to FINO3 data [Colour figure can be viewed at [wileyonlinelibrary.com](#)]

Comparing the result from the E10 model with the airborne measurements with a range of $1.80 \leq \alpha_{\text{obs}} \leq 6.60 \text{ h}^{-1}$, there is a suitable agreement for α_{FINO} . Especially for the MSO wake ($\alpha_{\text{obs}} = 3.60 \text{ h}^{-1}$), the observation matches with the analytical model. However, a difference in the wake recovery is indicated by the different farm layout (between AW and MSO by a factor of 4), which is not considered by the E10 model.

4.2 | Case study for Flight 30—August 8, 2017, morning

The data of the second case study were obtained from morning to noon on the same day, August 8, 2017, with the same flight pattern. Again, an easterly flow with wind speeds of about 10 m s^{-1} leads to distinct wakes behind AW, NO, and MSO. In contrast to the first case study, the stratification has a less stable to almost neutral gradient, with a thermal inversion at 160 m above sea level (see Figure 8). Thus, with the inversion at 160 m, the rotor blade area remains completely in the neutral layer.

4.2.1 | Flight data

Regarding the wind speeds of the undisturbed leg and the downwind zone (Figures 9 and 10A), a mesoscale variation with an acceleration of the flow from west to east in the range of 1 m s^{-1} exists. This increase is most likely ascribed to a land breeze, that accelerates over the smooth water surface.

FIGURE 9 Contour plot of the interpolated wind field measured during Flight 30 including the indication of the undisturbed wind field (gray dashed lines) and the wake boundaries (gray solid lines) [Colour figure can be viewed at wileyonlinelibrary.com]

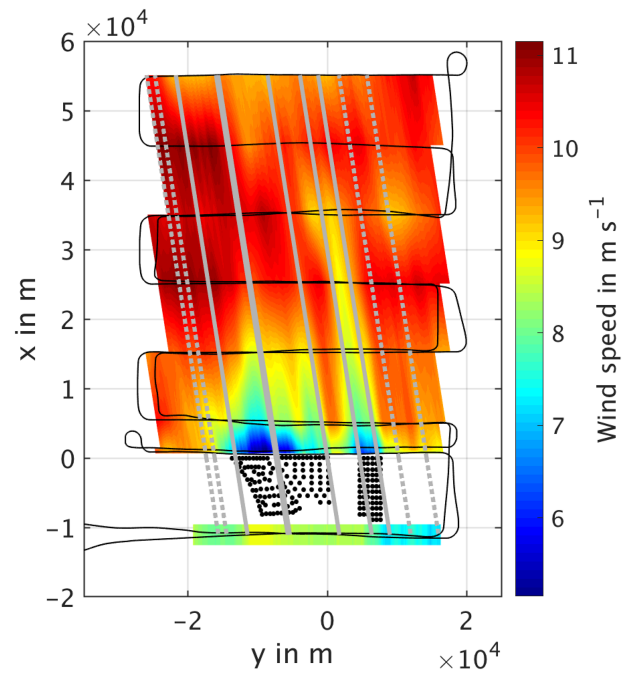
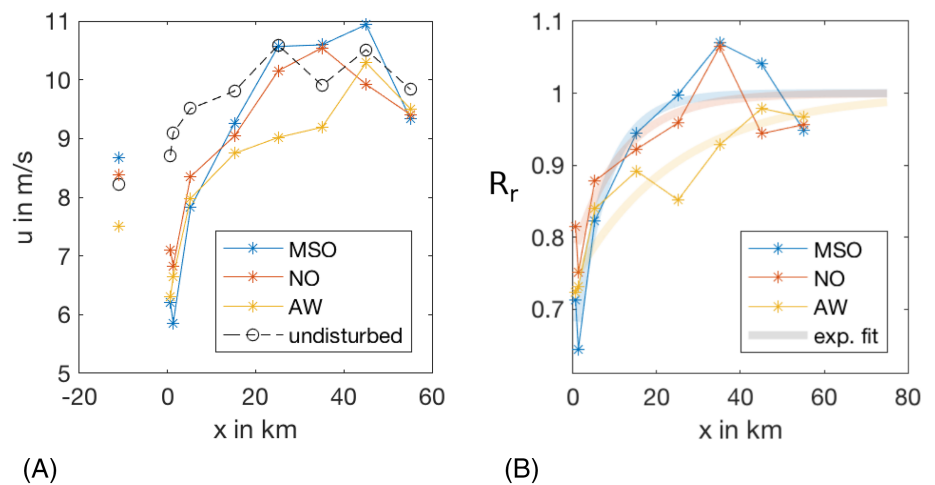


FIGURE 10 (A) As in Figure 5A but for Flight 30. (B) As in Figure 5B but for Flight 30 [Colour figure can be viewed at wileyonlinelibrary.com]



The observed wake recovery features spikes which are visible for all three evaluated wakes (Figure 10B). The wakes of the two adjacent farms MSO and NO are similar in their length (15–21 km). However, they differ significantly in the initial wind speed deficit, which is observed to be very high with 29% for MSO and only 19% for NO. In contrast, the wake of AW is significantly longer with 38 km or 76 min and with 28% initial deficit (Table 3). The approximation of the wake recovery with an exponential function seems to be as adequate as in the previous case study for Flight 31. The recovery rate of the fit a_{obs} ranging from 1.26 to 4.26 h^{-1} is lowest for the densest wind farm AW and highest for the farm MSO with a medium density.

4.2.2 | WRF model

With 6–8 m s^{-1} , the WRF model underestimates the wind speed compared to the measurements. The mean wind direction is estimated by the model with 90° which is about 10° higher than the observation. The thermal stratification is comparable to the measurements with an inversion at about 150 m above sea level and a neutral layer below. Between 9:00 to 11:00 UTC, however, a warming is modeled which has not been detected by the flight measurements.

The contour plots of the wake recovery in the WRF runs from 9:00 to 11:00 UTC are provided in Figure 11A–C. In all WRF runs, a strong wind speed gradient in north-east direction is evident, which has not been observed in the airborne data. This mesoscale background flow influences the result of R_r significantly. Thus, R_r is underestimated for MSO and overestimated for AW, where it even exceeds 1 (Figure 12A–C). In

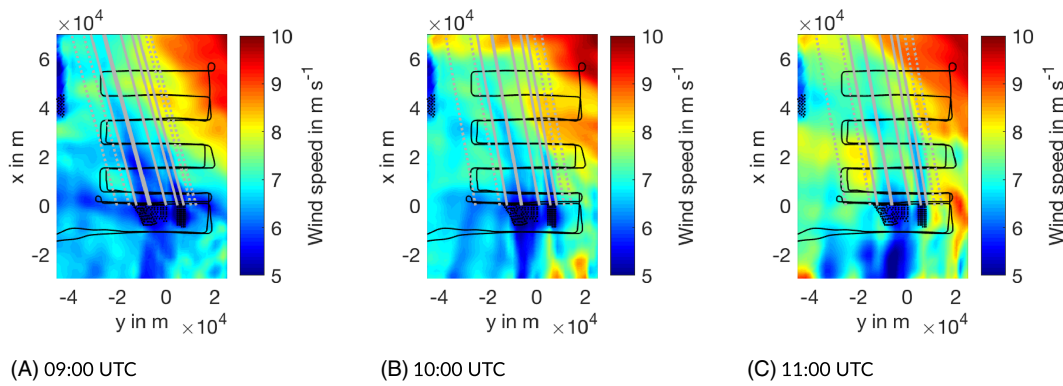


FIGURE 11 Wind speed contour plots and assigned wake boundaries of the WRF output for the case study 30 for different times of the simulation run [Colour figure can be viewed at wileyonlinelibrary.com]

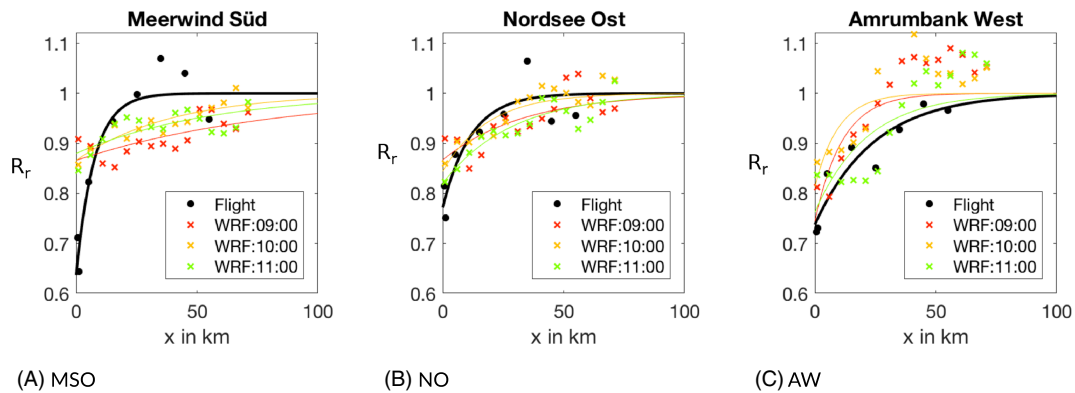


FIGURE 12 Relative wind speed deficit R_r in WRF behind the three wind farms MSO, NO and AW for case study of Flight 30. The solid line displays the best exponential fit of the airborne measurements. The red line shows the best fit of the WRF run at 09:00 UTC, the yellow at 10:00 UTC and green at 11:00 UTC [Colour figure can be viewed at wileyonlinelibrary.com]

summary, the model does not picture the measured recovery due to a different background wind field; nevertheless, the recovery rate modeled by WRF has still the same order of magnitude as the observation.

4.2.3 | E10 model

According to the WRF model, also a vertical separation Δz_{WRF} of 200 m is used for the E10 model for the case study of Flight 30. With the friction velocity $u_{* \text{FINO}} = 0.22 \text{ m s}^{-1}$ and $u_{* \text{profile}} = 0.26 \text{ m s}^{-1}$ being in the same range, this results in similar recovery rates by E10 of $\alpha_{\text{FINO}} = 2.32 \text{ h}^{-1}$ and $\alpha_{\text{profile}} = 2.81 \text{ h}^{-1}$ (Table 4). The analytical model is therefore in agreement with the observations of the wake recovery for the wind farm MSO ($\alpha_{\text{obs}} = 2.76 \text{ h}^{-1}$).

Concluding the case study of Flight 30, the observations and the analytical model show reasonable agreement. A comparison with the WRF model reveals that the mesoscale model does not reproduce the atmospheric conditions correctly. Therefore, the wake estimations do not agree with the observations and lead to misinterpretation of the wake recovery.

4.3 | Summary of further case studies

In addition to the two presented case studies, three further measurement flights with corresponding WRF modeling are evaluated and compared to the analytical model. Since the analysis method is very similar to the first two cases, only a brief summary of those studies is given.

4.3.1 | Case study for Flight 24

Summing up the analysis for Flight 24, stable atmospheric conditions are present during the measurement flight of the wake which was conducted on May 27, 2017, from 9:11 to 10:47 UTC. Extensive wakes exceeding 54 km or 117 min are observed downstream of AW and parts of the cluster NO/MSO (Figure 13A). The wake recovery can be described by an exponential fit with $\alpha_{\text{obs}} = 0.9 \text{ h}^{-1}$ (Figure 13B).

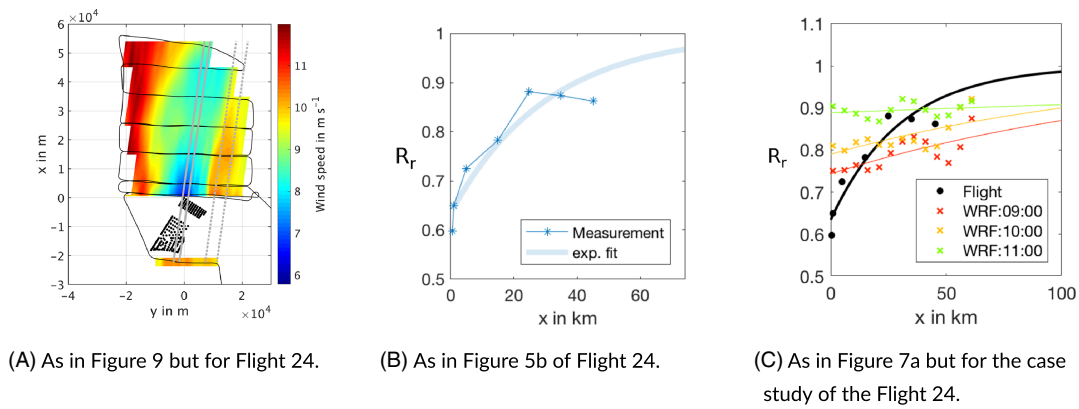


FIGURE 13 Wake extension for the case study of Flight 24 [Colour figure can be viewed at wileyonlinelibrary.com]

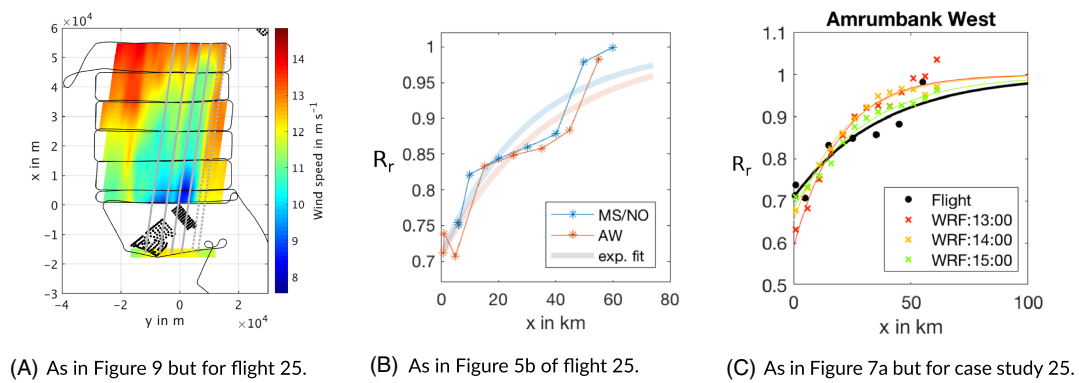


FIGURE 14 Wake extension for case study of Flight 25 [Colour figure can be viewed at wileyonlinelibrary.com]

The analytically estimated recovery rates ($\alpha_{\text{profile}} = 2.24 \text{ h}^{-1}$ and $\alpha_{\text{FINO}} = 1.78 \text{ h}^{-1}$) overestimate the observed one by a factor of about 2.

WRF simulations, with model runs of 9:00, 10:00, 11:00, and 12:00 UTC, underestimate the initial wind speed deficit. The recovery rate exhibits no exponential behavior (see Figure 13C). However, this is mainly because the atmospheric conditions are not estimated correctly since only the fourth run at 12 UTC represents a similar stable stratification as observed by the in situ data (not shown). The runs before 12 UTC show a neutral layer below 150 m with a small wake development.

4.3.2 | Case study for Flight 25

The case study for Flight 25 on May 27, 2017, provides wake measurements between 13:16 UTC and 14:55 UTC under relatively stationary, statically stable conditions. An internal boundary layer upstream of the wind farm with its top below the hub height grows above hub height with downstream distance. Moreover, a low level jet evolves with wind speeds exceeding 15 m s^{-1} . Wakes of about 50 km length (Figure 14A) are observed behind the wind farm cluster with an exponential recovery rate (best fit with RSME = 1.8) of approximately $\alpha_{\text{obs}} = 1.26 \text{ h}^{-1}$ (Figure 14B) for MSO/NO and 0.96 h^{-1} for AW. The recovery rate from the analytical model ($\alpha_{\text{profile}} = 1.72 \text{ h}^{-1}$ and $\alpha_{\text{FINO}} = 1.29 \text{ h}^{-1}$) is in the range of the observations.

The comparison of the observations and the WRF model runs at 13:00, 14:00, and 15:00 indicates that the height of the stable layer is overestimated in the model. However, WRF still reproduces the situation adequately. It only slightly underestimates the initial wind speed deficit and overestimates slightly the wake recovery with $1.20 < \alpha_{\text{WRF}} < 1.62 \text{ h}^{-1}$ (Figure 14C).

4.3.3 | Case study for Flight 7

During Flight 7 on September 9, 2016, slightly stable conditions were observed. The wake length is measured with 44 km or 104 min. A significant gradient of wind speed increase lateral to the flow was present (Figure 15A).

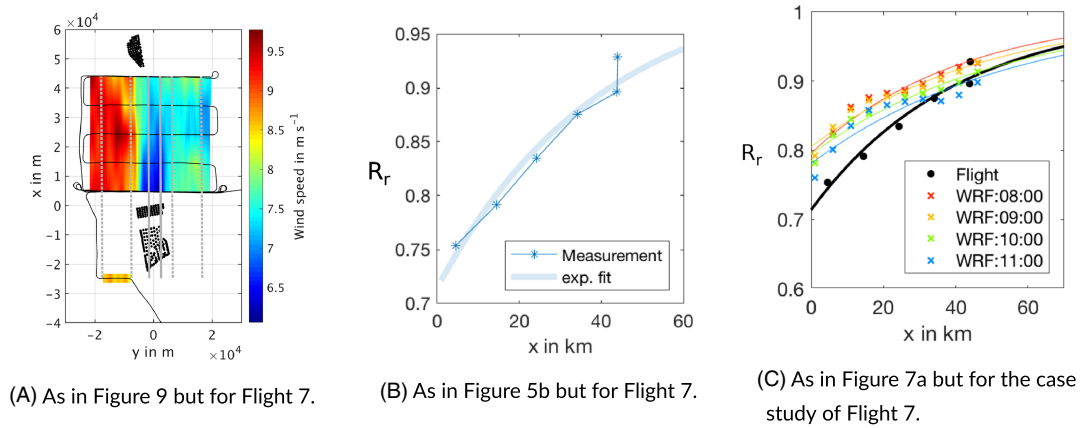


FIGURE 15 Wake extension for the case study of Flight 7 [Colour figure can be viewed at wileyonlinelibrary.com]

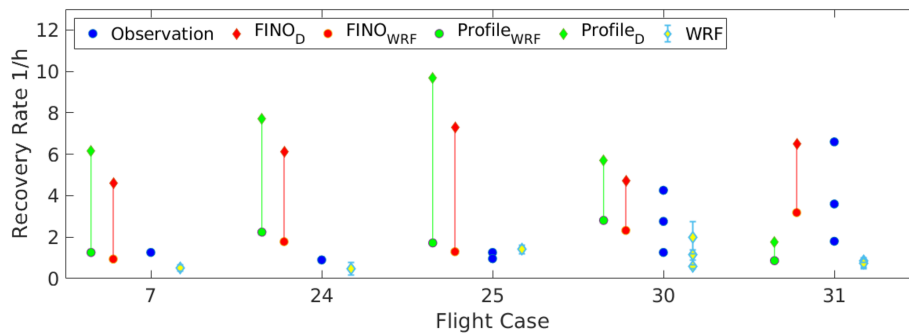


FIGURE 16 Overview of the recovery rates obtained for the five case studies. Blue dots are the observed ones (α_{obs}). Red and green dots are the recovery rates calculated by the E10 model either with u_{*FINO} or $u_{*profile}$. The range of the separation height between $\Delta z = D = 125$ m and $\Delta z = \Delta z_{WRF}$ is connected by a line. Recovery rates by the WRF model are indicated with a yellow-blue dot. The range between the minimum and maximum values of the different WRF model runs is marked with a bar [Colour figure can be viewed at wileyonlinelibrary.com]

The analysis shows that due to an indefinite background wind speed, the analytical model is sensitive toward such gradients. The effect is most prominent in the determination of the recovery rate α_{obs} , which ranges from 0.48 h^{-1} to 1.26 min^{-1} (Figure 15B) depending on the chosen reference background wind speed $u_f(x)$.

A comparison between the observations and the analytical exponential wake recovery model reveals that the analytical model agrees well with the observations ($\alpha_{FINO} = 3.18 \text{ h}^{-1}$), when using the sonic data from FINO1 to calculate u_* and is slightly lower when using the profile method ($\alpha_{profile} = 3.02 \text{ h}^{-1}$). The WRF simulation reproduces the atmospheric conditions well and underestimates the initial wind speed deficit only by less than 10%. However, the wake recovery is underestimated by WRF (Figure 15C) with α_{WRF} from 0.36 to 0.66 h^{-1} .

5 | COMPARISON AND DISCUSSION

The analysis of the five different cases shows that the E10 model can be used as a simple first-order approximation for the wake recovery downstream offshore wind farms with an exponential function as expected by Emeis.²³ Table 4 and Figure 16 present a summary of the recovery rate α obtained by the different methods: α_{obs} , which is observed by the airborne measurements, α_{FINO} and $\alpha_{profile}$, which is calculated by the E10 model using either the friction velocity u_{*FINO} by the FINO1 measurements or $u_{*profile}$ by the profile method, respectively. The E10 model reveals results in the same order of magnitude as the airborne observations and strengthens the hypothesis that the vertical downward moment flux has an important influence on the wake recovery. The best agreement of the wake recovery with a fitted exponential function is achieved for the case study of Flight 31 during stable and homogeneous wind conditions. However, not all wake-recovery curves exhibit such a distinct exponential behavior. In two case studies (Flights 24 and 25), the pattern can be interpreted to be more of a “step-wise” character which is indicated by a higher RMSE when fitting an exponential function. This may also be related to the assumption that the atmospheric conditions do not change. However, the meander pattern is measured in a time span of over 1 h and temporal changes are likely and may influence the results.

All values of the observations and the corresponding WRF simulations have the same order of magnitude if the maximum value of the WRF simulation α_{WRFmax} is considered, except for the measured wake downstream NO of Flight 31. The best match of WRF model and the

observations is achieved for case study of Flight 25 and shows further adequate results in the case study of Flight 31. For the other cases, results from the WRF model are not very suitable for a precise size estimation of α , as the simulation of the wake extension deviates due to different simulated atmospheric conditions.

The deviation between simulations and observation is rooted in an underestimation of the temperature on land. The stable conditions described herein resulted all from offshore winds advecting warm air over a cold North Sea. The simulations tended to underestimate the temperature on land compared to the observations. Hence, too cold air was advected over the North Sea in the simulations resulting in less stable conditions as observed. As the atmospheric conditions drive the length of the wake, the model failed to describe the wakes reasonably in such cases.

Both methods for the estimation of the friction velocity u_* give similar results (see Table 4 and Figure 16), although for the cases of Flights 31, 24, and 25, u_* obtained by the profile method and hence the recovery rate α_{profile} slightly overestimates the observations. The case of Flight 31, however, is an exception. Here, the profile method reveals four to five times smaller value of u_* , since the measured Monin-Obukhov z/L (as explained in Section 4.1) is not representative for the surface layer in this case. It should be noted that for the calculation of u_* (Equation 9), the roughness length is set to $z_0 = 0.0001$ m for all cases. A variation of the length between $z_0 = 0.001$ m and $z_0 = 0.00001$ m will change the results of the recovery rate α in the range of about maximum 30% and should be considered, but cannot explain a factor of 4–5.

A main drawback of the analytical E10 model is that vertical separation between the hub height and the undisturbed flow Δz is rather difficult to estimate, which has been already mentioned by Peña and Rathmann.³⁵ As in this study no measured data for the separation height are available, estimations of Δz by the WRF simulations were used. However, this should be considered only as a rough estimation. Cañadillas et al.³⁶ assumed that the separation height equals the rotor diameter D of the wind turbine. For the case studies with the wind farm cluster AW/MSO/NO, $\Delta z = D$ is approximately 125 m. For a comparison, the recovery rate α by the E10 model using $\Delta z = D = 125$ m, in addition to the estimates by the WRF, runs $\Delta z = \Delta z_{\text{WRF}}$ (Table 4 and Figure 16). The results indicate an overestimation of the recovery rate α using the separation height D . This implies that larger length scales than D must be considered over which the vertical exchange occurs, and it has to be further assumed that the separation height Δz is not a constant value along the wake.

Several studies^{22,37–39} showed that the wake intensity within the wind farm depends crucially on the wind direction and the farm layout: a higher wake loss or a larger initial wind speed deficit is observed when the wind direction is parallel to the turbine rows and the turbines are aligned. The opposite case would be a staggered layout; here, lower wake losses are observed. The in situ data prove that a denser wind farm layout leads to a larger initial wind speed deficit.

However, this effect would only explain a change in the initial wind speed deficit, not the impact on the wake recovery downstream of the farm itself. The E10 proposes that the recovery rate depends solely on the wind speed deficit behind the wind farm and the atmospheric stability, expressed by the friction velocity u_* and Δz . In other words, this means that for the same atmospheric conditions, the recovery rate is expected to be constant and independent of the wind farm layout as the model already includes the wind speed deficit D_{r1} caused by the wind farm. With the case study of Flights 30 and 31, we can check this hypothesis as distinct wakes are visible behind the single wind farms AW, MSO, NO within the same atmospheric conditions, but with different farm layout.

The results show, however, that a clear influence by the farm layout is evident. Most prominent is the impact in the case study of Flight 31. The relationship is observed that the wake length and duration as well as the initial wind speed D_{r1} increase with the wind farm density from NO over MSO to AW. In contrast, the recovery rate decreases. In the case study of Flight 30, likewise the lowest recovery rate and the longest wake are observed for the densest farm AW. A possible explanation is that the theory is based on the fact that the wind farm has an infinite lateral dimension. Therefore, a possible explanation that not only a vertical momentum flux but also a horizontal flux from the sides is present, which erodes the wind speed deficit in the wake faster for narrow than for wide wakes. It is expected that a more loose wind farm allows a stronger horizontal flux. However, this hypothesis could not be proven with this data set.

A further aspect which is not considered by the E10 model is the influence of the wind farms itself on the turbulence and the atmospheric stratification. The model uses the friction velocity u_* , which is obtained in the undisturbed flow. Due to the production of turbulence by the wind turbines,^{38,40,41} a modification of the atmospheric stability (e.g., u_*) by forming a farm-induced internal boundary layer (IBL) is expected,¹⁸ although as shown by Siedersleben,⁴² who investigated how wind farms change turbulent fluxes and stability, a general statement in his study was not possible. Emeis¹⁷ took the wind farm generated turbulence intensity into account to estimate a modified wind speed deficit D_{r1} by an extension of the E10 model. Besides that however, the results also indicate that the wind farm generated turbulence has an influence on the separation height and the friction velocity depending on the wind farm layout. This feature should be implemented by an extension of the analytical model.

6 | CONCLUSION AND OUTLOOK

The wake recovery of offshore wind farm wakes was analyzed by in situ data, measured with the research aircraft Dornier DO-128 during the WIPAFF project in 2016 and 2017. This unique data set was used to validate the analytical model E10 by Emeis²³ for five case studies. Moreover, the recovery rates were compared with the results of the mesoscale WRF model.

The measured data demonstrate that the velocity deficit downstream of offshore wind farms can be approximated by a simple analytical wake model using an exponential recovery. The recovery rates calculated by the E10 model showed comparable results to the observations.

Based on the measurements, the wind farm layout was identified to influence the resulting wake recovery, which has only been considered indirectly and not sufficiently by the E10 model.

During stable atmospheric conditions, a difference in the wake length of up to 30 km was observed downstream farms with a different layout, a difference of up to 10% for the initial wind speed deficit and differences in the recovery rate by a factor of up to 4. The case study of the Flights 30 and 31 showed that the denser the turbines in the wind farm, the longer is the wake and the lower the recovery rate. This variance of the recovery rate has not been represented by the model results. As the E10 model is based on the assumption that the wake recovery is controlled only by the vertical momentum flux, it is suggested that not only a vertical momentum flux but also a horizontal flux from the sides is present and coheres with factors such as the farm width and the wind direction and take into account the wind farm produced turbulence.

Also, some drawbacks have to be considered in this study. The assumption is made that the atmospheric conditions are stationary during the measurements. Measuring the full extent of the wake by the aircraft takes a time span of over 1 h, and temporal changes in the atmospheric conditions are likely.

Furthermore, wake meandering is not considered with the assumption of a linear development along the mean wind direction. The analysis could be extended to non-linear wake extension, following the path of lowest wind speed downstream of the wind farms and therefore also improve the choice of boundary between the wake and the undisturbed wind field. Also, a wind speed gradient perpendicular to the wind direction influences the results crucially. A variable background speed, for example, evaluated over a linear regression perpendicular to the wind direction may improve the result but would increase the complexity of the evaluation^{36,43} and may cause new inaccuracies.

For the future, more measurements are needed for a stronger statement. Right now, the study is based on five case studies only. Further examination should also include less stable and more convective cases for better universality. Simultaneous flights with a manned aircraft for the wake extent and small unmanned aircraft systems (UAS)⁴⁴⁻⁴⁶ for the measurement of vertical profiles inside and downwind of the wind farm in order to obtain the vertical wind profiles could serve for a better estimation of the separation height Δz between the decelerated wind field and the undisturbed flow. The results in this study indicate that separation height Δz should be considered larger than the wind turbine rotor diameter as assumed by Cañadillas et al.,³⁶ at least at the beginning of the wake. In addition, it should be examined whether Δz changes along the wake.

ACKNOWLEDGEMENTS

The authors thank the crew of the WIPAFF campaign, Rudolf Hankers, Thomas Feuerle, Helmut Schulz, and Mark Bitter for their support. The project WIPAFF was funded by the German Federal Ministry for Economic Affairs and Energy (Bundesministerium für Wirtschaft und Energie) on the basis of a decision by the German Bundestag grant number: FKZ 0325783. FINO data were provided by the BSH with the support by the BMWi (Bundesministerium für Wirtschaft und Energie) and PTJ (Projekträger Jülich).

PEER REVIEW

The peer review history for this article is available at <https://publons.com/publon/10.1002/we.2568>.

ORCID

Andreas Platis  <https://orcid.org/0000-0002-9276-3587>

Jens Bange  <https://orcid.org/0000-0003-4075-1573>

REFERENCES

1. BWE-Bundesverband-Windenergie. https://www.energy-charts.de/power_inst.htm?year=2020%26period=annual%26type=power_inst; 2019.
2. Fraunhofer-ISE. Net installed electricity generation capacity in Germany in 2020. https://www.energy-charts.de/power_inst.htm?year=2020period=annual%26type=power_inst; 2020.
3. Emeis S, Siedersleben S, Lampert A, et al. Exploring the wakes of large offshore wind farms. *J Phys Conf Ser.* 2016;753(9):92014.
4. Henderson AR, Morgan C, Smith B, Sørensen HC, Barthelmie RJ, Boesmans B. Offshore wind energy in Europe—a review of the state-of-the-art. *Wind Energy: An Int J Progress Appl Wind Power Conversion Technol.* 2003;6(1):35-52.
5. Nygaard NG, Hansen SD. Wake effects between two neighbouring wind farms. *J Phys Conf Ser.* 2016;753(3):32020.
6. Emeis S. Current issues in wind energy meteorology. *Meteorol Appl.* 2014;21(4):803-819.
7. Platis A, Siedersleben SK, Bange J, et al. First in situ evidence of wakes in the far field behind offshore wind farms. *Sci Rep.* 2018;8(1):2163.
8. Christiansen MB, Hasager CB. Wake effects of large offshore wind farms identified from satellite SAR. *Remote Sens Environ.* 2005;98(2-3):251-268.
9. Li X, Lehner S. Observation of TerraSAR-X for studies on offshore wind turbine wake in near and far fields. *IEEE J Sel Top Appl Earth Observ Remote Sens.* 2013;6(3):1757-1768.
10. Djath B, Schulz-Stellenfleth J, Cañadillas B. Impact of atmospheric stability on X-band and C-band synthetic aperture radar imagery of offshore windpark wakes. *J Renew Sustain Energy.* 2018;10(4):43301.
11. Platis A, Bange J, Bärfuss K, et al. Long-range modifications of the wind field by offshore wind parks—results of the project WIPAFF. *Meteorologische Zeitschrift.* 2020. <https://doi.org/10.1127/metz/2020/1023>

12. Crespo A, Hernandez J, Frandsen S. Survey of modelling methods for wind turbine wakes and wind farms. *Wind Energy: An Int J Progress Appl Wind Power Conv Technol*. 1999;2(1):1-24.
13. Lissaman SP. Energy effectiveness of arbitrary arrays of wind turbines. *J Energy*. 1979;3(6):323-328.
14. Jensen NO. *A note on wind generator interaction*. Citeseer; 1983.
15. Newman BG. The spacing of wind turbines in large arrays. *Energy Conv*. 1977;16(4):169-171.
16. Frandsen S. On the wind speed reduction in the center of large clusters of wind turbines. *J Wind Eng Indust Aerodyn*. 1992;39(1-3):251-265.
17. Emeis S. *Wind Energy Meteorology: Atmospheric Physics for Wind Power Generation*. Springer; 2018.
18. Porté-Agel F, Bastankhah M, Shamsoddin S. Wind-turbine and wind-farm flows: a review. *Bound-Layer Meteorol*. 2020;174(1):1-59.
19. Lundquist JK, DuVivier KK, Kaffine D, Tomaszewski JM. Costs and consequences of wind turbine wake effects arising from uncoordinated wind energy development. *Nat Energy*. 2019;4(1):26-34.
20. Siedersleben SK, Lundquist JK, Platis A, et al. Micrometeorological impacts of offshore wind farms as seen in observations and simulations. *Environ Res Lett*. 2018;13(12):124012.
21. Fitch AC, Olson JB, Lundquist JK, et al. Local and mesoscale impacts of wind farms as parameterized in a mesoscale NWP model. *Monthly Weather Rev*. 2012;140(9):3017-3038.
22. Frandsen S, Barthelmie R, Pryor S, et al. Analytical modelling of wind speed deficit in large offshore wind farms. *Wind Energy: An Int J Progress Appl Wind Power Conv Technol*. 2006;9(1-2):39-53.
23. Emeis S. A simple analytical wind park model considering atmospheric stability. *Wind Energy*. 2010;13(5):459-469.
24. Corsmeier U, Hankers R, Wieser A. Airborne turbulence measurements in the lower troposphere onboard the research aircraft Dornier 128-6, D-IBUF. *Meteorologische Zeitschrift*. 2001;10(4):315-329.
25. Lampert A, Bärfuss K, Platis A, et al. In situ airborne measurements of atmospheric and sea surface parameters related to offshore wind parks in the German Bight. *Earth Syst Sci Data*. 2020;12(2):935-946.
26. Foreman RJ, Cañadillas B, Neumann T, Emeis S. Measurements of heat and humidity fluxes in the wake of offshore wind turbines. *J Renew Sustain Energy*. 2017;9(5):53304.
27. Stull RB. *An Introduction to Boundary Layer Meteorology*, Vol. 13: Springer Science & Business Media; 2012.
28. Paulson CA. The mathematical representation of wind speed and temperature profiles in the unstable atmospheric surface layer. *J Appl Meteorol*. 1970;9(6):857-861.
29. Högström ULF. Non-dimensional wind and temperature profiles in the atmospheric surface layer: a re-evaluation. *Topics in Micrometeorology. A Festschrift for Arch Dyer*. Dordrecht: Springer; 1988:55-78.
30. Charnock H. Wind stress on a water surface. *Quart J R Meteorol Soc*. 1955;81(350):639-640.
31. Garratt JR. Review of drag coefficients over oceans and continents. *Monthly Weather Rev*. 1977;105(7):915-929.
32. Nakanishi M, Niino H. An improved Mellor-Yamada level-3 model with condensation physics: its design and verification. *Bound-Layer Meteorol*. 2004;112(1):1-31.
33. Siedersleben SK, Platis A, Lundquist JK, et al. Evaluation of a wind farm parametrization for mesoscale atmospheric flow models with aircraft measurements. *Meteorologische Zeitschrift*. 2018;27.
34. Siedersleben SK, Platis A, Lundquist JK, et al. Observed and simulated turbulent kinetic energy (WRF 3.8. 1) overlarge offshore wind farms. *Geosci Model Development Discuss Rev*. 2020:1-29.
35. Peña A, Rathmann O. Atmospheric stability-dependent infinite wind-farm models and the wake-decay coefficient. *Wind Energy*. 2014;17(8):1269-1285.
36. Cañadillas B, Foreman R, Barth V, et al. Offshore wind farm wake recovery: airborne measurements and its representation in engineering models. *Wind Energy*. 2020;23(5):1249-1265.
37. Porté-Agel F, Lu H, Wu Y-T. Interaction between large wind farms and the atmospheric boundary layer. *Procedia Iutam*. 2014;10:307-318.
38. Porté-Agel F, Wu Y-T, Chen C-H. A numerical study of the effects of wind direction on turbine wakes and power losses in a large wind farm. *Energies*. 2013;6(10):5297-5313.
39. Barthelmie RJ, Hansen K, Frandsen ST, et al. Modelling and measuring flow and wind turbine wakes in large wind farms offshore. *Wind Energy: An Int J Progress Appl Wind Power Conv Technol*. 2009;12(5):431-444.
40. Frandsen ST. Turbulence and turbulence-generated fatigue loading in wind turbine clusters. *Report Draft Form Ris*. 2005.
41. Hansen KS, Barthelmie RJ, Jensen LE, Sommer A. The impact of turbulence intensity and atmospheric stability on power deficits due to wind turbine wakes at Horns Rev wind farm. *Wind Energy*. 2012;15(1):183-196.
42. Siedersleben S. Numerical analysis of offshore wind farm wakes and their impact on the marine boundary layer. *Universität zu Köln*. 2019.
43. Bodini N, Zardi D, Lundquist JK. Three-dimensional structure of wind turbine wakes as measured by scanning lidar. *Atmos Measure Techn*. 2017;10(8).
44. Van den Kroonenberg A, Martin T, Buschmann M, Bange J, Vörsmann P. Measuring the wind vector using the autonomous mini aerial vehicle M²AV. *J Atmos Ocean Technol*. 2008;25(11):1969-1982.
45. Platis A, Altstädter B, Wehner B, et al. An observational case study on the influence of atmospheric boundary-layer dynamics on new particle formation. *Bound-Layer Meteorol*. 2016;158(1):67-92.
46. Rautenberg A, Schön M, zum Berge K, et al. The multi-purpose airborne sensor carrier MASC-3 for wind and turbulence measurements in the atmospheric boundary layer. *Sensors*. 2019;19(10):2292.

How to cite this article: Platis A, Hundhausen M, Mauz M, et al. Evaluation of a simple analytical model for offshore wind farm wake recovery by in situ data and Weather Research and Forecasting simulations. *Wind Energy*. 2020;1-17. <https://doi.org/10.1002/we.2568>